

Finite Element Analysis of RC Tapered Beams under Cyclic Loading

Ibrahim S. I. Harba
College of Engineering
Al- Nahrain University
ibraharba@yahoo.com

Abdulkhalik J. Abdulridha
College of Engineering
Al- Nahrain University
abdulkalikjabbar@yahoo.com

Abstract

This paper presents a numerical investigation to study the effect of variations in displacement history sequence and magnitude on cyclic response of RC tapered (haunched) beams (RCHBs). Five simply supported RCHBs (four haunched and one prismatic) were selected from experimental work carried out by Aranda et al. The selected variables included were five loading history types. The first part of this study focused to verify the finite element analysis with selected experimental work and the second part of this study focused too studying the effect of varying in loading history to the response of RCHBs. The finite element code Abaqus was used in the modeling. The adopted cyclic simulation performance of the selected beams using the plastic- damage model for concrete developed by Lubliner and Lee & Fenves. The constitutive model of plain concrete describing the uniaxial compression response under cyclic loading proposed by Thorenfeldt, and the uniaxial tension response follows the softening law proposed by Hordijk was used in the modeling. Menegotto-Pinto model was used to simulate the steel response. Model verification has shown A good agreement to the selected experimental work. The variations in loading history will decrease the ultimate load and corresponding deflection with increase in the number of cycles at ultimate load.

1. Introduction

Reinforced concrete tapered or haunched beams (RCHBs) have been used around the world for design, bridges and buildings [1]. Therefore, in this paper a five simply supported RCHBs tested by Aranda *et al.* are designed to fail in shear under monotonic loading [1] were modeled by using nonlinear finite elements. The first part of this study focused on capability of a constitutive modeling of simulating the behavior of RCHBs under cyclic reversed shear loading against experimental data. The parametric study was conducted to determine the response to various cyclic shear loading histories applied for each specimen; the ability of the modeling to capture the strength, stiffness degradation, shear strength, and failure mechanisms (e.g. cracking patterns) was demonstrated as the second part of this study.

The finite element code Abaqus was used in the modeling. A plastic damage model originally developed by Lubliner et al. [2] and later extended by Lee and Fenves [3]. This model captures the failure of concrete by representing the evolving strength of concrete using a hyperbolic approximation of the Drucker-Prager failure surface coupled with a continuum damage mechanics approach for stiffness degradation. This model is available in Abaqus.

The constitutive model of plain concrete describing the uniaxial compression response under cyclic loading proposed by Thorenfeldt [4], and the uniaxial tension response follows the softening law proposed by Hordijk [5] was used in the modeling. In this paper, the additional components necessary to simulate reinforced concrete are determined to ensure the simulation compatibility against experimental data, and steel reinforcing bar response, i.e. ,the Bauschinger effect where in the reinforcing bars exhibit premature yielding during load reversals. Menegotto-Pinto [6] model was used to simulate the steel response.

2. Description of the Experimental Study

The geometry, boundary conditions and loads used in the experimental program by Aranda et al. [1] were also used for the finite element models are shown in Figure(1). All RCHBs specimens have a total length $L = 330$ cm. The effective span for all RCHBs was $L = 2.80$ m and the width was $b = 22$ cm. The considered angles of slope of the haunch from horizontal were: 0° , 3.07° , 6.12° , 9.13° and 12.10° . The haunched length at both beam ends was one-third the effective span of the beam ($L_h = L/3 = 93.3$ cm). The bearing length at both beam ends was 25 cm. The linear tapering was obtained by keeping a constant depth $h_{max} = 45$ cm at the beam ends while varying the depth of the beam at the central third from 45 cm (prismatic) to 25 cm, that is, $h_{min} = 45, 40, 35, 30$ and 25 cm. Beams were simply supported and tested under cyclic reversed loads (F) that were applied 10 cm (3.937 in.) from the vertex formed by the intersection of tapered sections with the prismatic section, as depicted in Figure (1). The cryptogram used for the identification for the

RCHBs, $HB\alpha$, where α is an index that indicates the considered haunched angle. Flexural and shear reinforcement details for each beam considered in

the experimental program are shown in Figure (2). Also, the corresponding typical cross sections are shown in Figure (3).

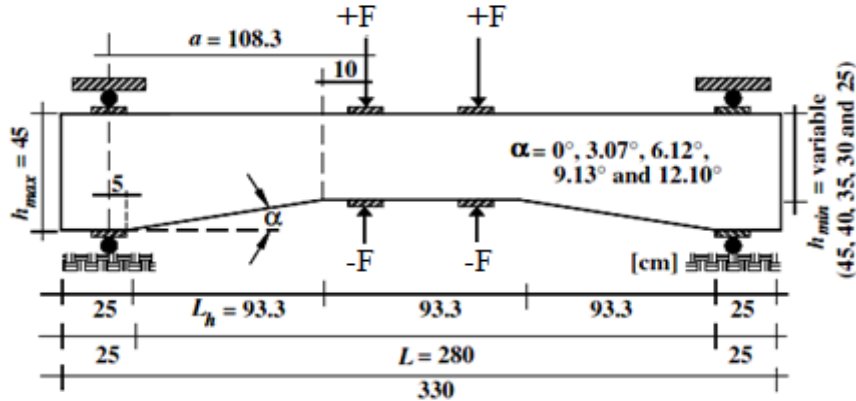
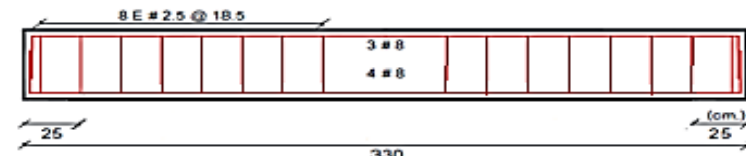
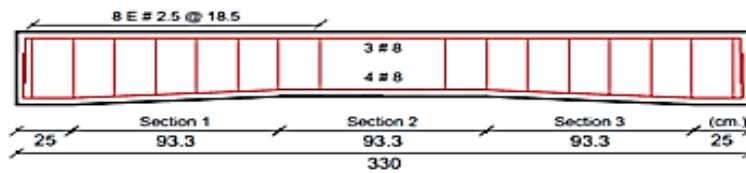


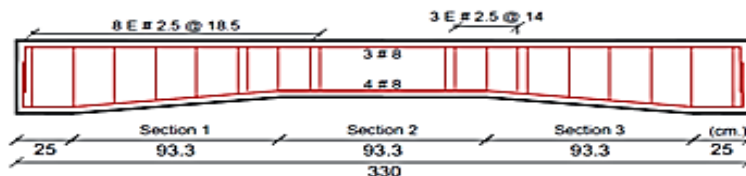
Figure (1): Geometry, boundary conditions and loads [1].



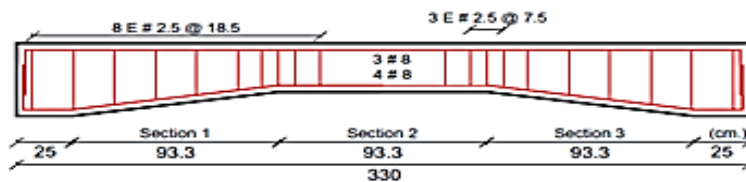
(a) HB0



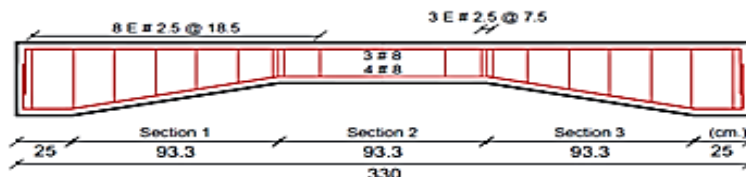
(b) HB 3.07



(c) HB 6.12



(d) HB 9.13



(e) HB 12.10

Figure (2): Steel reinforcement detail [1].

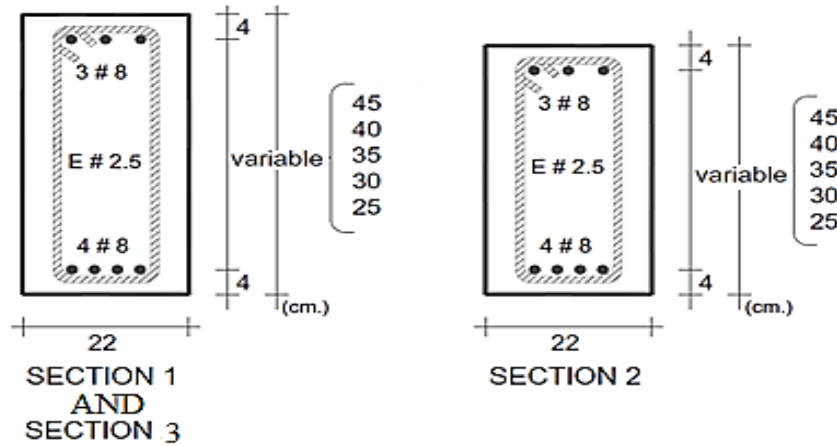


Figure (3): Typical cross sections [1].

3. Material Constitutive Model

In order to study the effect of variations in displacement history sequence and magnitude on cyclic behavior of RC haunched beams, the numerical study is conducted. The input data for modeling the material finite element program ABAQUS to obtain the hysteretic behavior of concrete is used from experiment and test results [1].

3.1. Concrete Constitutive Model

The concrete constitutive behavior is simulated using plasticity based damage model with three-dimensional continuum [7]. The method is efficiently capable of simulating concrete in all types of elements. Inelastic performance of concrete is conducted by using the isotropic damaged elasticity concept with isotropic of compressive and tensile plasticity [2, 3, 8]. The formula proposed by Thorenfeldt [4] is adopted to calculate the stress-strain relationship of uniaxial compression response of concrete under cyclic loading and associated parameters are given as:

$$\sigma = f'_c \left(\frac{\epsilon}{\epsilon_0} \right)^{\frac{n}{n-1 + \left(\frac{\epsilon}{\epsilon_0} \right)^{nk}}} \quad (1)$$

$$n = 0.8 + \frac{f'_c}{17} \quad (2)$$

$$k = \begin{cases} 1.0 & \epsilon_0 > \epsilon \\ 0.67 + \frac{f'_c}{62} \geq 1.0 & \epsilon_0 < \epsilon \end{cases} \quad (3)$$

In this equation, f'_c is the reported compressive strength and ϵ_0 is the strain corresponding to the maximum compressive value and is taken as 0.002, which Thorenfeldt [4] specifies as:

$$\epsilon_0 = \frac{f'_c}{E_c} \cdot \frac{n}{n-1} \quad (4)$$

Unless experimental values are reported for a particular set of experimental data, the elastic modulus for concrete is evaluated according to the ACI [9] equation as:

$$E_c = 4700 \sqrt{f'_c} \text{ (MPa)} \quad (5)$$

The general shape of Thorenfeldt's uniaxial compression model is illustrated in Figure (4), in which the analytical expression from Equation (1) is verified with ABAQUS implementation of the model.

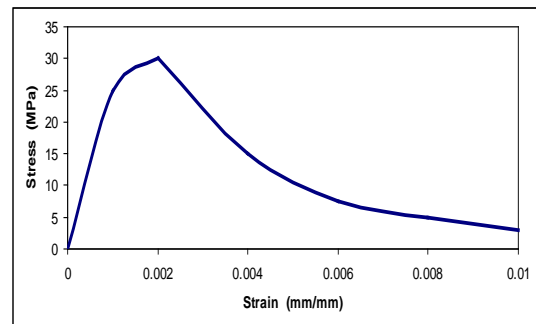


Figure (4): Thorenfeldt [4] concrete compression analytical curve.

The concrete stress-strain performance in compression is chosen up to $0.4 f'_c$ as linearly elastic. The considered plastic strain is defined beyond this region.

Linear-elastic behavior of concrete in tension is assumed until the uniaxial tensile stress, at which concrete cracks. These assumptions are used in the finite element modeling to define the stress and strain of concrete. The uniaxial tension response proposed by Hordijk [5], expressed as:

$$\sigma_{cr} = f_t \left[\left(1 + \left(c_1 \frac{\epsilon_{cr}}{\epsilon_{ult}} \right)^3 \right) e^{\left(c_2 \frac{\epsilon_{cr}}{\epsilon_{ult}} \right)} - \frac{\epsilon_{cr}}{\epsilon_{ult}} (1 + c_1^2) e^{-c_2} \right] \quad (6)$$

$$\epsilon_{ult}^{cr} = 5.136 \frac{G_f}{h f_t} \quad (7)$$

Where " $c_1 = 3$ and $c_2 = 6.93$ also the strain ϵ_{ult}^{cr} represents the maximum inelastic strain value for which tensile stresses are developed, which depends on the mode-I fracture energy G_f and tensile strength f_t ". The crack bandwidth h is a characteristic length providing mesh objectivity with respect to the fracture energy G_f . When concrete is modeled using solid elements, the crack bandwidth is taken as $\sqrt[3]{V}$ where V is the volume of the element [7]. For beam and truss elements, the default value of h is taken as the length of the element. The tensile strength f_t is computed according to the CEB-FIP Model Code 1990 [10] as:

$$f_t = 0.3 (f_c')^{2/3} \tag{8}$$

While the fracture energy G_f is computed according to the equation proposed by Rimmel [11] as:

$$G_f = 0.065 \cdot \ln \left(1 + \frac{f_c'}{10} \right) \quad (N/mm) \tag{9}$$

The general features of Hordijk's uniaxial tension model are illustrated in Figure (5), in which the analytical expression from Equation (6) is verified with ABAQUS implementation of the model.

Moreover, Figure (6) explains the concrete cyclic behavior with the transition phenomenon of load. At the start, a linear behavior of material up to the failure of tensile stress σ_{t0} ; representing the onset of micro-cracking in the concrete.

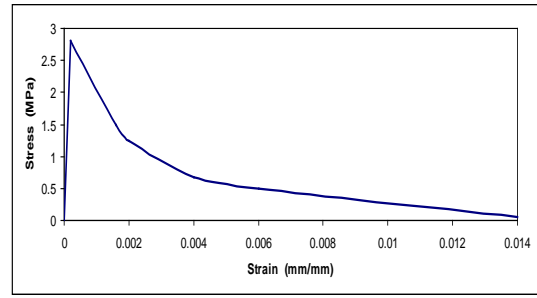


Figure (5): Hordijk [5] tension softening analytical curve.

The strain softening mechanism of the cracked concrete is start after this stress and the material propagates towards. The failure performance is defined using stress strain post failure relation modeled by TENSION STIFFENING as the more pronounced effects in the tension side. The simple simulation of concrete steel interaction effects is also supported by this phenomenon [7]. During the processes of unloading and reloading, the concrete elastic stiffness is damaged, i.e. the transition of load from tension to compression. The damage variables where " d_t and d_c ($0 \leq d_t, d_c \leq 1$) describes the degradation of elastic stiffness". The closing and opening of earlier formed cracks due to cyclic loadings, this reason makes the degradation mechanism become complex. When the load changes sign, the stiffness recovery occur since the material is recover some of elastic stiffness due to closing of tensile cracks extensively which causes this recovery. The recovery is characterizes by the value of tension damage variable (d_t). The initial elastic stiffness E_0 reduction is usually expressed by the following expression:

$$E = (1 - d_t)E_0 \tag{10}$$

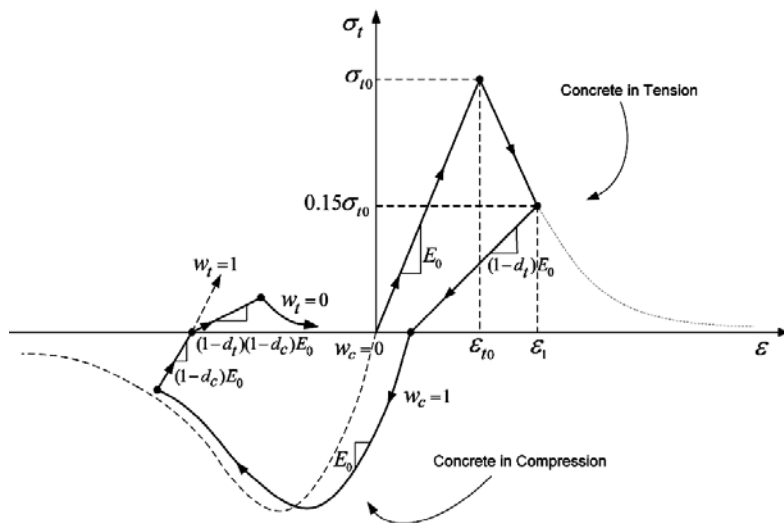


Figure (6): Concrete cyclic behavior [7].

Through the load reversal, the compressive and tensile stiffness recovery is defined by factors w_t and w_c . The set of values for these factors were as default i.e. $w_t=0$ and $w_c=1$. The material regain full stiffness with no damage when a unit compression recovery factor w_c is used. While no stiffness recovery occurs when zero values of w_c was used. On the other hand, no recover of tensile stiffness during tension loading. The compression damage d_c is denoted by the factor w_t . The behavior of compression is depicted as an input by the COMPRESSION HARDENING data as a function of inelastic strain rate. The direction of plastic strain in the yield surface defined with a dilation angle of 37° . To give more realistic of concrete behavior, the mechanical properties of concrete (tensile strength, Poisson's ratio, elastic modulus and plastic strains) are defined according to concrete compressive test results [2, 3].

3.2. Steel Reinforcement Constitutive Model

The behavior of RC haunched beams is dependent on the nonlinear cyclic response of reinforcing bars. The Bauschinger effect where in the reinforcing bars exhibit premature yielding during load reversals as shown in Figure (7), since the modified unloading/reloading curves allow cracks to close more easily during load reversals and thus improve the compression zone performance. Analytical models for reinforcing bar response in this study were used steel models incorporating the Bauschinger effect was Menegotto-Pinto [6]. Menegotto and Pinto [6] proposed an analytical model capable of representing the hysteretic behavior of steel reinforcing bars exhibiting the Bauschinger effect together with isotropic strain hardening. The Menegotto-Pinto model is available in ABAQUS for embedded reinforcements [7]. In this model, the constitutive response consists of one-dimensional stress-strain relations for branches between two subsequent load reversal points, and is expressed in terms of dimensionless stress σ^* and strain ϵ^* as:

$$\sigma^* = b\epsilon^* + \frac{(1-b)\epsilon^*}{(1+\epsilon^{*R})^{\frac{1}{R}}} \quad (11)$$

Where " b is the ratio of the strain hardening to initial modulus and R is the curvature parameter controlling the shape of the unloading-reloading cycles", defined as:

$$R = R^0 - \frac{A_1 \epsilon_p^{\max}}{A_2 + \epsilon_p^{\max}} \quad (12)$$

In this equation " R^0 is the initial curvature parameter and ϵ_p^{\max} is the maximum plastic excursion during a previous half-cycle". Isotropic hardening is represented by the equation:

$$\frac{\sigma_{sh}}{\sigma_{y0}} = A_3 \cdot \left(\frac{\epsilon_{max}^t}{\epsilon_{y0}} - A_4 \right) \quad (13)$$

Where " σ_{y0} and ϵ_{y0} are the initial yield stress and corresponding strain, ϵ_{max}^t is the maximum absolute total strain at the instant of strain reversal, and σ_{sh} is the stress shift in the linear yield asymptote for isotropic hardening". A_1 to A_4 are material constants which require experimental determination. A parameter study, together with recommendations from the literature [6, 12], led to a selection of these parameters as $b = 0.002$, $R^0 = 22.0$, $A_1 = 18.5$, $A_2 = 0.15$, $A_3 = 0.15$ and $A_4 = 0.0$.

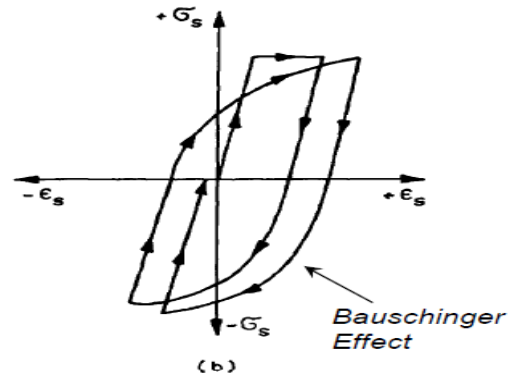


Figure (7): Repeated reverse cyclic loading.

4. Material Properties

The experimental material properties of the steel reinforcement, steel plate, and concrete are shown in Table (1). Also the five simply supported RCHBs tested by Aranda et al. [1] are shown in Table (2).

Table (1): Measured experimental properties for the steel reinforcement [1].

| Bar number | $f_y(\sigma_{y0})$ kg/cm ² (MPa) | ϵ_y | $f_{sh}(\sigma_{sh})$ kg/cm ² (MPa) | f_u kg/cm ² (MPa) |
|------------|---|--------------|--|--------------------------------|
| 8 | 4348 (426.5) | 0.00237 | 4348 (426.5) | 7707 (756.1) |
| 2.5 | 4592 (450.5) | 0.00235 | 4592 (450.5) | 7436 (729.5) |

Table (2): Measured experimental shear forces and characteristic displacements of cyclic tests [1].

| Beam symbol | α (degree) | f'_c (MPa) | V_{cr} (kN) | V_u (kN) | Δ_{cr} (mm) | Δ_u (mm) | Number of Cycle |
|-------------|-------------------|--------------|---------------|------------|--------------------|-----------------|-----------------|
| HB0 | 0 | 22.3 | 44.7 | 244.2 | 4.14 | 20.14 | 9 |
| HB3.07 | 3.07 | 24 | 80.2 | 203.6 | 8.04 | 24.42 | 11 |
| HB6.12 | 6.12 | 21.3 | 60.4 | 129.8 | 8 | 20.02 | 9 |
| HB9.13 | 9.13 | 27.9 | 28.6 | 134.4 | 4.06 | 29.29 | 13 |
| HB12.10 | 12.10 | 24 | 14.9 | 77.3 | 4.08 | 33.92 | 15` |

Where:

α =haunch angle

f'_c = cylinder concrete compressive strength.

V_{cr} , Δ_{cr} = first diagonal shear force and corresponding mid span deflection.

V_u , Δ_u = ultimate diagonal shear force and corresponding mid span deflection.

5. Parametric Study

The loading history was considered to be the most important variable in this investigation to study the effect of variations in displacement history sequence and magnitude on cyclic response of RC haunched beams. The five types of loading

history included in this study were selected to study the effect of changes in the size of maximum displacements and changes in the sequence of application of large and small mid span displacements on RC haunched beams behavior. These loading histories, designated as Types (1) through (5), are shown schematically in Figure (8).The load history Type 1 represent the experimental program by Aranda et al. [1] to calibrate the finite analysis with experimental results before implementation they remain loading histories.

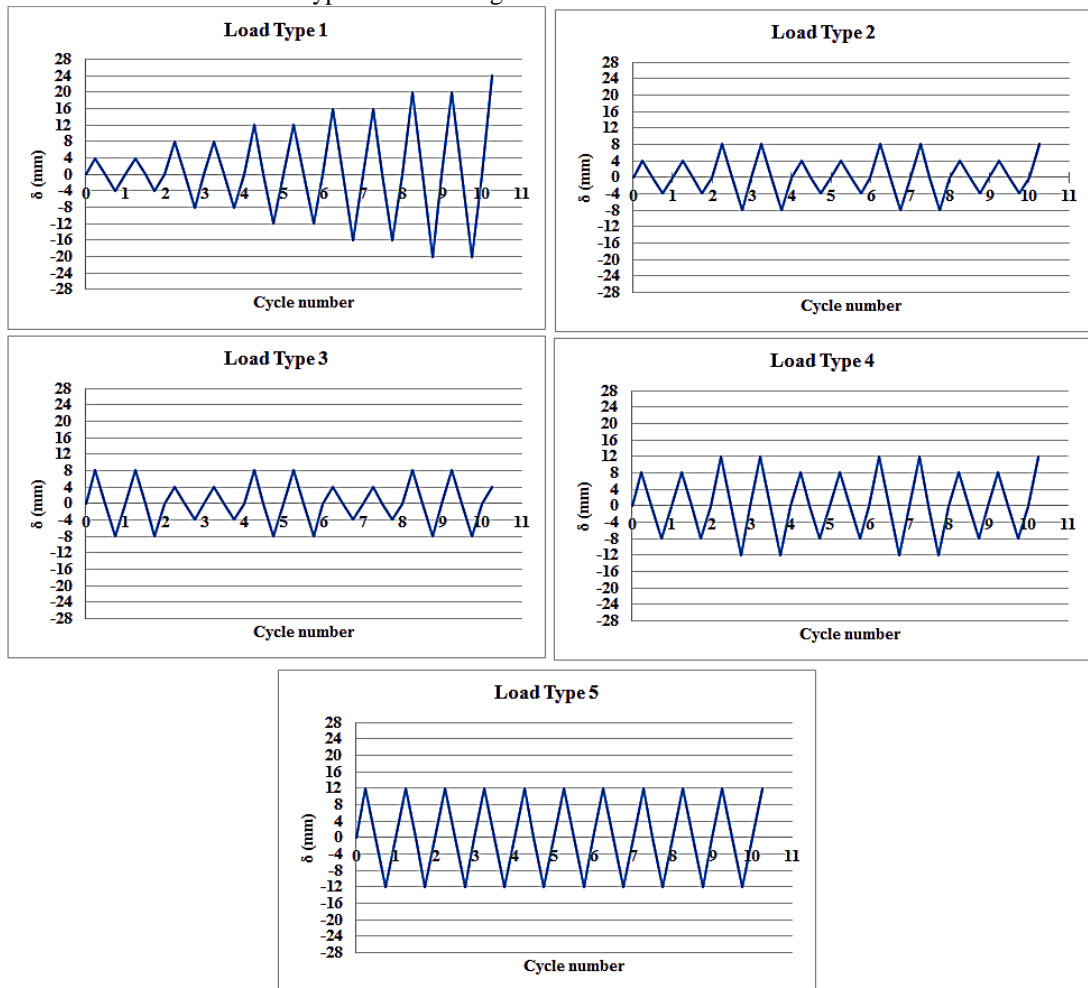


Figure (8): Load histories types.

6. Finite Element Type, Mesh and Loading

In this study to simulate the behavior of the investigated beams, the concrete and steel bearing plate elements were modeled by using solid elements, in order to be more efficient in defining the boundaries of the elements and modeling the behavior. A fine mesh of three-dimensional eight-node solid elements C3D8 [13, 14] was used. A sketch of the finite element model is shown in Figure (9). Such elements necessitate a denser mesh for accurate and efficient simulations. On the other hand, although using a reduced integration the model gets essentially stiffer, the parameters of tension stiffening are necessary to be adjusted to match proper experimental values

[15, 16]. The T3D2 (A 2- node linear 3D truss) elements are used to model the steel reinforcement. The finite element types are shown in Figure (10).

Two methods of loading are generally used for numerical analysis: (1) the application of force F ($F = V$ shear force); or (2) the application of displacement Δ . In this study, the loading applied by incremental increasing of displacement. This method was preferred for consistency with the experimental procedure in which the test specimens were loaded under displacement control, as well as for convergence issues. The reaction forces give the external loads and the failure load was obtained by plotting the shear-displacement response.

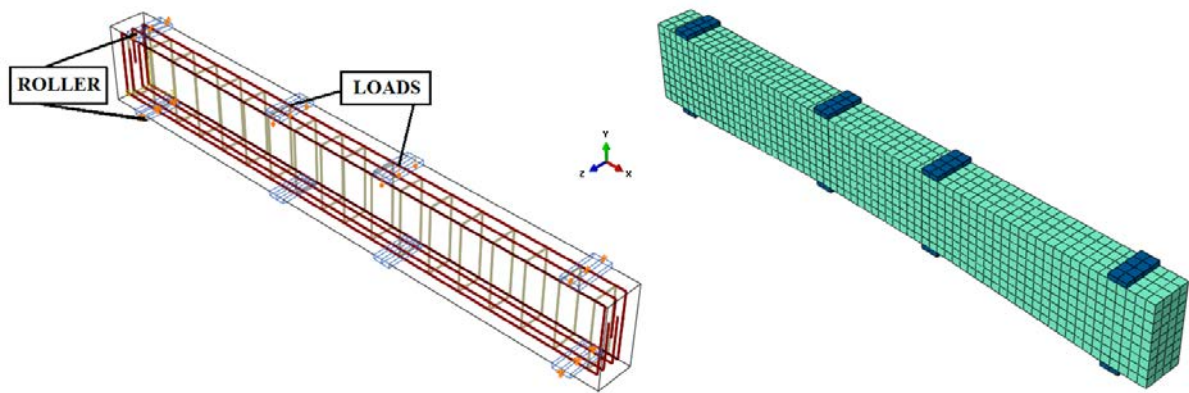


Figure (9): A sketch of the finite element model.

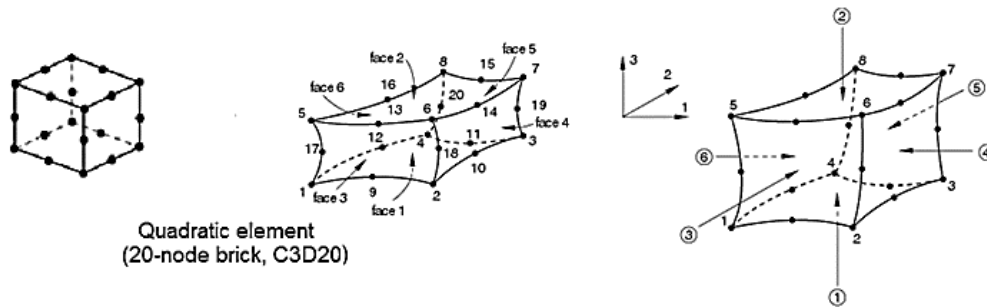


Figure (10): The finite element types [7].

7. Analysis Results and Discussions

The numerical studies are performed to predict the capability of a constitutive modeling of simulating the behavior of RCHBs under cyclic reversed shear loading compared with the experimental values, as mentioned earlier as first part of this study. This was carried out by applying load history Type 1 which represents the experimental program by Aranda et al. [1] to calibrate the finite element analysis with experimental results. the second part of this study

are performed to predict the response of RCHBs under various cyclic shear loading histories by applying load histories Type 2, Type 3, Type 4, and Type 5 for each specimens. The results from the numerical analysis are the values of the shear force–deflection at mid span, and ultimate loads, the numerical results are shown in Table (3). The hysteretic loops and the overall skeleton curves are used to present and validate out comes. The crack patterns associated with maximum plastic strain (Damages) are also presented.

Table (3): Numerical analysis results.

| Beam Designation | First Plastic* Strain Deflection Δ_{cr} (mm) | First Plastic Strain Shear Load V_{cr} (kN) | Ultimate Deflection Δ_u (mm) | Ultimate Shear Load V_u (kN) | Number of Cycle |
|------------------|---|---|-------------------------------------|--------------------------------|-----------------|
| HB0T1 | 4.18 | 46.3 | 20.4 | 238.4 | 10 |
| HB3.07T1 | 4.53 | 50.5 | 22.54 | 236.5 | 10 |
| HB6.12T1 | 3.52 | 35.4 | 19.5 | 126.7 | 9 |
| HB9.13T1 | 4.13 | 27.4 | 30.6 | 143.1 | 12 |
| HB12.10T1 | 4.72 | 22.1 | 31.2 | 110.2 | 12 |
| HB0T2 | 4.2 | 45.3 | 9.91 | 223.1 | 15 |
| HB3.07T2 | 4.21 | 57.4 | 21.48 | 221.3 | 15 |
| HB6.12T2 | 3.33 | 32.5 | 23.3 | 119.4 | 15 |
| HB9.13T2 | 4.15 | 25.6 | 35.8 | 124.4 | 15 |
| HB12.10T2 | 4.19 | 21.0 | 29.6 | 86.4 | 15 |
| HB0T3 | 4.12 | 43.8 | 9.32 | 245.4 | 15 |
| HB3.07T3 | 4.01 | 50.4 | 22.71 | 217.8 | 15 |
| HB6.12T3 | 3.50 | 34.1 | 21.7 | 136.2 | 15 |
| HB9.13T3 | 4.05 | 28.8 | 36.4 | 130.8 | 15 |
| HB12.10T3 | 4.13 | 19.3 | 29.8 | 89.2 | 15 |
| HB0T4 | 4.19 | 44.4 | 12.4 | 232.4 | 14 |
| HB3.07T4 | 4.36 | 51.4 | 18.14 | 241.3 | 15 |
| HB6.12T4 | 3.54 | 34.5 | 24.16 | 146.4 | 15 |
| HB9.13T4 | 4.09 | 26.3 | 37.65 | 114.1 | 15 |
| HB12.10T4 | 4.02 | 19.6 | 38.2 | 93.4 | 15 |
| HB0T5 | 4.08 | 45.0 | 14.3 | 229.0 | 15 |
| HB3.07T5 | 4.14 | 54.3 | 16.87 | 189.5 | 13 |
| HB6.12T5 | 3.62 | 38.8 | 18.1 | 99.9 | 13 |
| HB9.13T5 | 4.11 | 27.8 | 32.2 | 139.4 | 15 |
| HB12.10T5 | 3.99 | 20.9 | 30.9 | 91.4 | 15 |

*First plastic strain deflection Δ_{cr} recorded when first plastic strain occurs in ABAQUS software program for each specimen.

7.1 Comparison between Numerical and Experimental Results

In this section, comparisons between the experimental data [1] and the finite element results from ABAQUS models are presented.

7.1.1 Shear Force Mid-span Deflection and Ultimate Load Capacity

The shear force - mid span deflection obtained from numerical simulation of specimens under load type 1 are compared in Figure (11) and Table (4) with those obtained experimentally. As it can be observed in Figure (11), that there are differences between numerical and experimental curves, since in experimental test after impose the load in positive and negative directions in the process of loading and unloading there will be a residual deflection so that to avoid this problem they retrain the measure of LVDT to zero after loading and unloading but in the finite element this is not possible so that the final ultimate shear force and corresponding deflection in the experimental and numerical analysis refer to a good correlation of hysteretic loops exists for the five beam specimens. Table (4) shows a comparison between numerical results predicted

by finite element software ABAQUS for load histories type 1 and experimental results [1]. The ultimate shear load (V_u) from numerical analysis is decreased by 4 percent (in average) and the corresponding ultimate mid span deflection (Δ_u) is increased by 3 percent (in average) than experimental values. While the numerical first cracking shear load (V_{cr}) (first plastic strain) and the corresponding mid span deflection (Δ_{cr}) are decreased by 19.5 and 37.6 percent respectively (in average) than experimental values.

The numerical number of cycles at ultimate load decreased by 33 percent (in average) than experimental values. It can be seen that ABAQUS can be basically consistent with the experimental test results, but there are also differences between the values calculated by the numerical analysis and the test. The reason may be the following [17]:

- 1) Finite element simulations is assumed to have a uniform, isotropic and the same contact form between cells, however, the constitution of actual concrete is very complex, including cement, sand, gravel and so on. The Complicated action between them cannot be easily replaced by unified form.

2) In Finite Element Analysis, bond between concrete and steel is processed using the Embedded Technology, effectively simplifying the modeling, but it cannot be achieved with the increased load of reinforced concrete and changing nature of the friction moment, especially reinforced slip simulation. This can easily lead to distorted results.

3) Other factors also affect the results of the analysis such as convergence of Finite Element Analysis, reasonableness of simulation parameter values, form and quantity of finite element division and casting quality and loading conditions of specimens test.

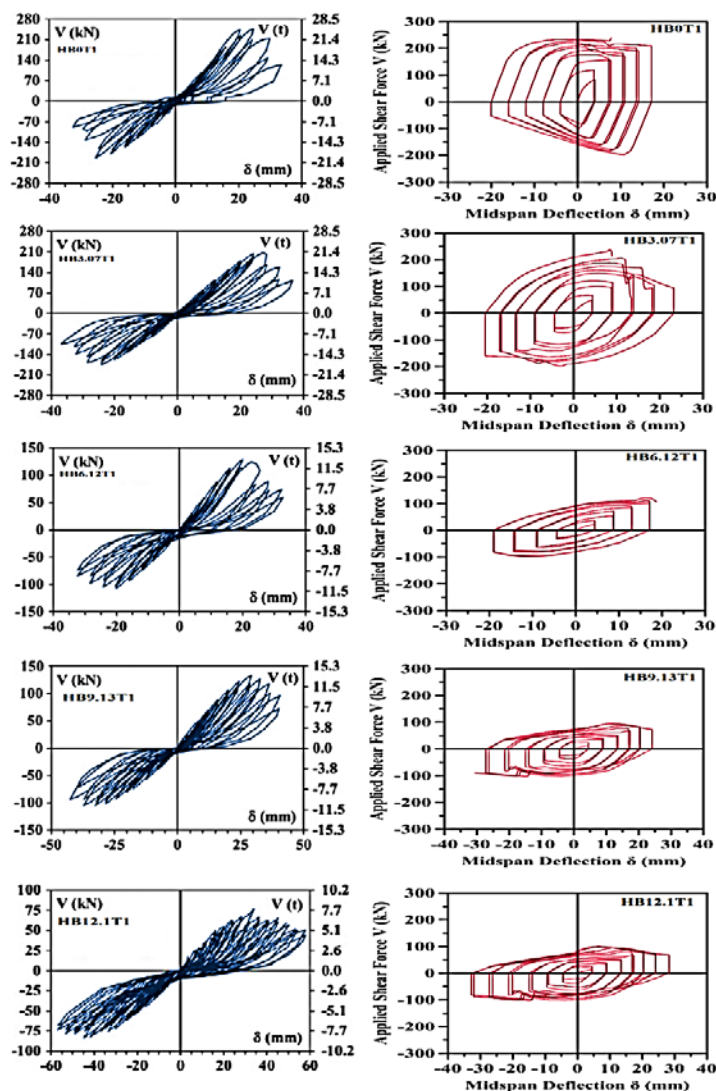


Figure (11): Experimental and numerical hysteretic curves for control beams tested under (load history 1).

Table (4): Comparison between numerical and experimental results for load histories type 1.

| Beam Designation | $\Delta_{cr} \text{ EXP} / \Delta_{cr} \text{ NUM}$ | $V_{cr} \text{ EXP} / V_{cr} \text{ NUM}$ | $\Delta_u \text{ EXP} / \Delta_u \text{ NUM}$ | $V_u \text{ EXP} / V_u \text{ NUM}$ | NO. of Cycle. EXP / NO. of Cycle. NUM |
|------------------|---|---|---|-------------------------------------|---------------------------------------|
| HB0T1 | 0.990431 | 0.965443 | 0.987255 | 1.024329 | 0.9 |
| HB3.07T1 | 1.774834 | 1.588119 | 1.083407 | 0.860888 | 1.1 |
| HB6.12T1 | 2.272727 | 1.706215 | 1.026667 | 1.024467 | 1 |
| HB9.13T1 | 0.983051 | 1.043796 | 0.95719 | 0.939203 | 1.083333 |
| HB12.10T1 | 0.864407 | 0.674208 | 1.087179 | 0.701452 | 1.25 |

7.1.2 Cracking Patterns and Damages

ABAQUS model predicts cracks propagation during loading cycles in tension and in compression faces of the specimens. The numerical cracking patterns at ultimate load compared with experimental cracks patterns as shown in Figure (12), indicates a good correlation between experimental and numerical results. Figure (13) shows the damages (plastic strain in concrete at ultimate load). The contour plots of the modeled specimens in Blue color indicates concrete's in elastic behavior, other colors regions indicates formation of microcracks until beginning of concrete yield, orange color defines concrete contains cracks and red color defines full concrete failure. Based upon the observed numerical cracks patterns and damages which

were very well predicted using ABAQUS model, it can be noted that the development of a plastic hinge zone was found to be in the middle of the haunch length ($1/2 L_h$) and this response is well estimated compared to the experimental results. These discussions indicates that the numerical load-carrying capacity, mid span deflections and failure behavior of RCHBs under cyclic reversed shear loading compared with the experimental values [1] to calibrate the finite element analysis can be simulated with good accuracy . Also these results allowed to predict the response of RCHBs under various cyclic shear loading histories as the second part of this study using the adopted numerical analysis method.

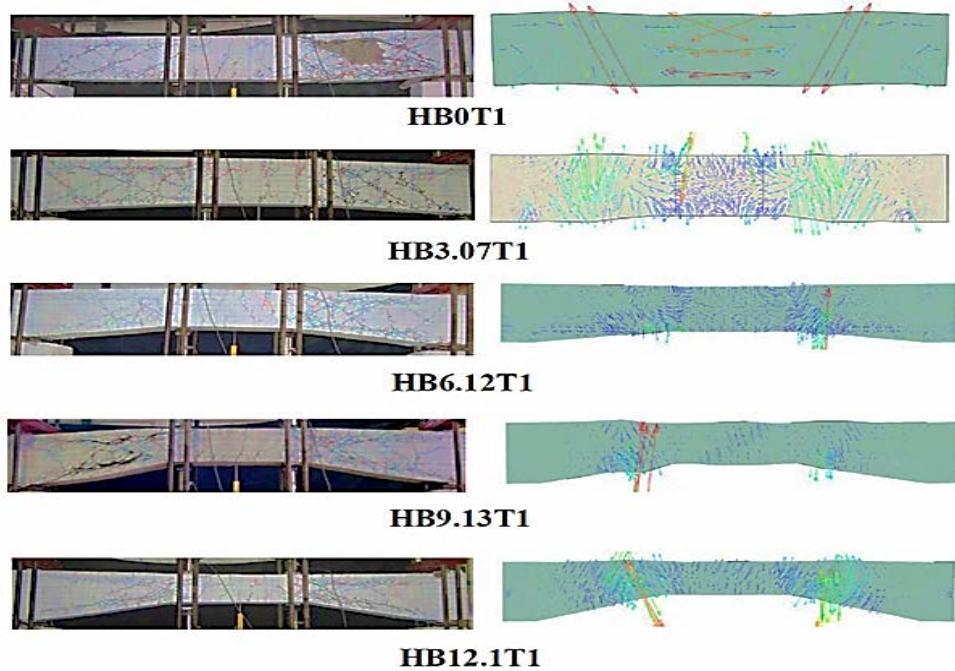


Figure (12): Experimental and numerical crack patterns for load type 1.

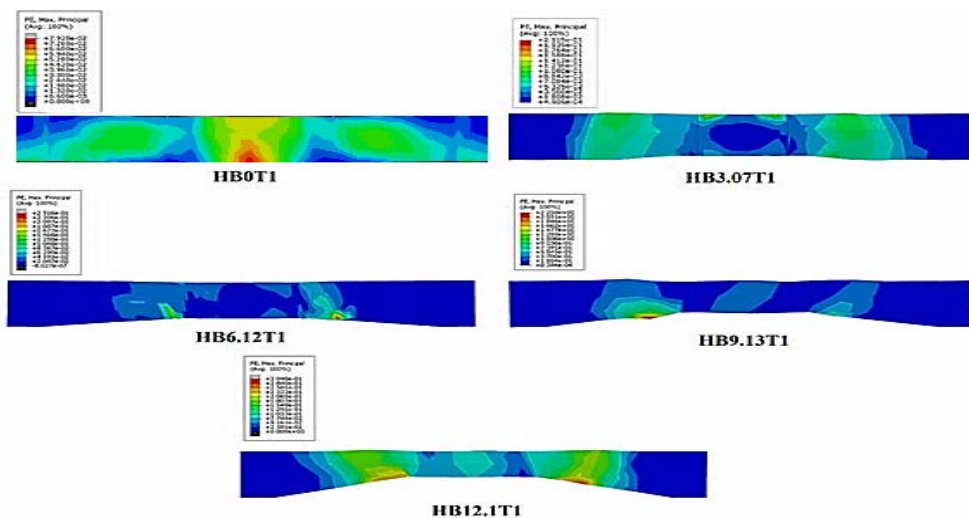


Figure (13): Numerical plastic strain in concrete at ultimate load for load type 1.

7.2 Effects of Variations of Loading History

In this section, the effects of variations in loading history to the response of RCHBs under various cyclic shear loading histories are presented. Also a comparisons between load histories Type 1, Type 2, Type 3, Type 4, and Type 5 for each specimen are also presented as shown in Table (5) and Figure (14). The shear force - mid span deflection obtained from numerical simulation of specimens under various cyclic shear loading histories (Type 2, Type 3, Type 4, and Type 5) are presented in Figures (15 to 18). In general, it can be observed in Figures (15 to 18) and Table (5), there are no significant change in the numerical first cracking shear load (V_{cr}) (first plastic strain) and the corresponding mid span deflection (Δ_{cr}) for the five beam specimens under various loading histories (Tn) (where n=Type 2, Type 3, Type 4, and Type 5) compared to load histories Type 1. While a significant change in the ultimate shear load (V_u) from numerical analysis for various loading histories is decreased by 7.9 percent (in average) and the corresponding

ultimate mid span deflection (Δ_u) is decreased by 5.52 percent (in average) compared to load histories Type 1. The numerical number of cycles at ultimate load for various loading histories increased by 46 percent (in average) compared to load histories Type 1.

Based upon the observed numerical cracks patterns and damages from Figures (18 to 25) for the five beams which predict a similar cracks patterns and damages compared to five beams under load histories Type 1, as shown in Figures (11 and 12). Also, it can be noted from Figures (18 to 25) that the development of a plastic hinge zone were found also in the middle of the haunch length ($1/2 L_h$). The discussions indicates that the differences in sequence of application of large and small displacements for various cyclic shear loading histories (Type 1, Type 2, Type 3, Type 4, and Type 5) did not cause a significant difference in overall response of RCHBs. Figures (19 to 22) shows the crack pattern and Figures (23 to 26) shows and damages (plastic strain in concrete at ultimate load) for various loading histories (Type 2, Type 3, Type 4, and Type 5).

Table (5): Numerical results for all load histories types.

| Beam Designation | $\Delta_{cr}T_n/\Delta_{cr}T_1$ | $V_{cr}T_n/V_{cr}T_1$ | Δ_uT_n/Δ_uT_1 | V_uT_n/V_uT_1 | NO. of Cycle.Tn/ NO. of Cycle.T1 |
|------------------|---------------------------------|-----------------------|---------------------------|-----------------|----------------------------------|
| HB0T1 | 1 | 1 | 1 | 1 | 1 |
| HB0T2 | 1.00478469 | 0.9784 | 0.48578 | 0.93582 | 1.52632 |
| HB0T3 | 0.9856 | 0.946 | 0.4568 | 1.0293 | 1.526 |
| HB0T4 | 1.00239234 | 0.95896 | 0.60784 | 0.97483 | 1.42105 |
| HB0T5 | 0.97607656 | 0.97192 | 0.70098 | 0.96057 | 1.57895 |
| HB3.07T1 | 1 | 1 | 1 | 1 | 1 |
| HB3.07T2 | 0.92935982 | 1.13663 | 0.95297 | 0.93573 | 1.57895 |
| HB3.07T3 | 0.88520971 | 0.99802 | 1.00754 | 0.92093 | 1.57895 |
| HB3.07T4 | 0.96247241 | 1.01782 | 0.80479 | 1.0203 | 1.52632 |
| HB3.07T5 | 0.91390728 | 1.07525 | 0.74845 | 0.80127 | 1.31579 |
| HB6.12T1 | 1 | 1 | 1 | 1 | 1 |
| HB6.12T2 | 0.94602273 | 0.91808 | 1.19487 | 0.94238 | 1.76471 |
| HB6.12T3 | 0.99431818 | 0.96328 | 1.11282 | 1.07498 | 1.76471 |
| HB6.12T4 | 1.00568182 | 0.97458 | 1.23897 | 1.15549 | 1.76471 |
| HB6.12T5 | 1.02840909 | 1.09605 | 0.92821 | 0.78848 | 1.52941 |
| HB9.13T1 | 1 | 1 | 1 | 1 | 1 |
| HB9.13T2 | 1.00484262 | 0.93431 | 1.16993 | 0.86932 | 1.30435 |
| HB9.13T3 | 0.98062954 | 1.05109 | 1.18954 | 0.91405 | 1.30435 |
| HB9.13T4 | 0.99031477 | 0.95985 | 1.23039 | 0.89588 | 1.30435 |
| HB9.13T5 | 0.99515738 | 1.0146 | 1.24837 | 0.97414 | 1.30435 |
| HB12.10T1 | 1 | 1 | 1 | 1 | 1 |
| HB12.10T2 | 0.88771186 | 0.95023 | 0.94872 | 0.78403 | 1.30435 |
| HB12.10T3 | 0.875 | 0.8733 | 0.95513 | 0.80944 | 1.30435 |
| HB12.10T4 | 0.85169492 | 0.88688 | 1 | 0.84755 | 1.30435 |
| HB12.10T5 | 0.84533898 | 0.9457 | 0.99038 | 0.8294 | 1.30435 |

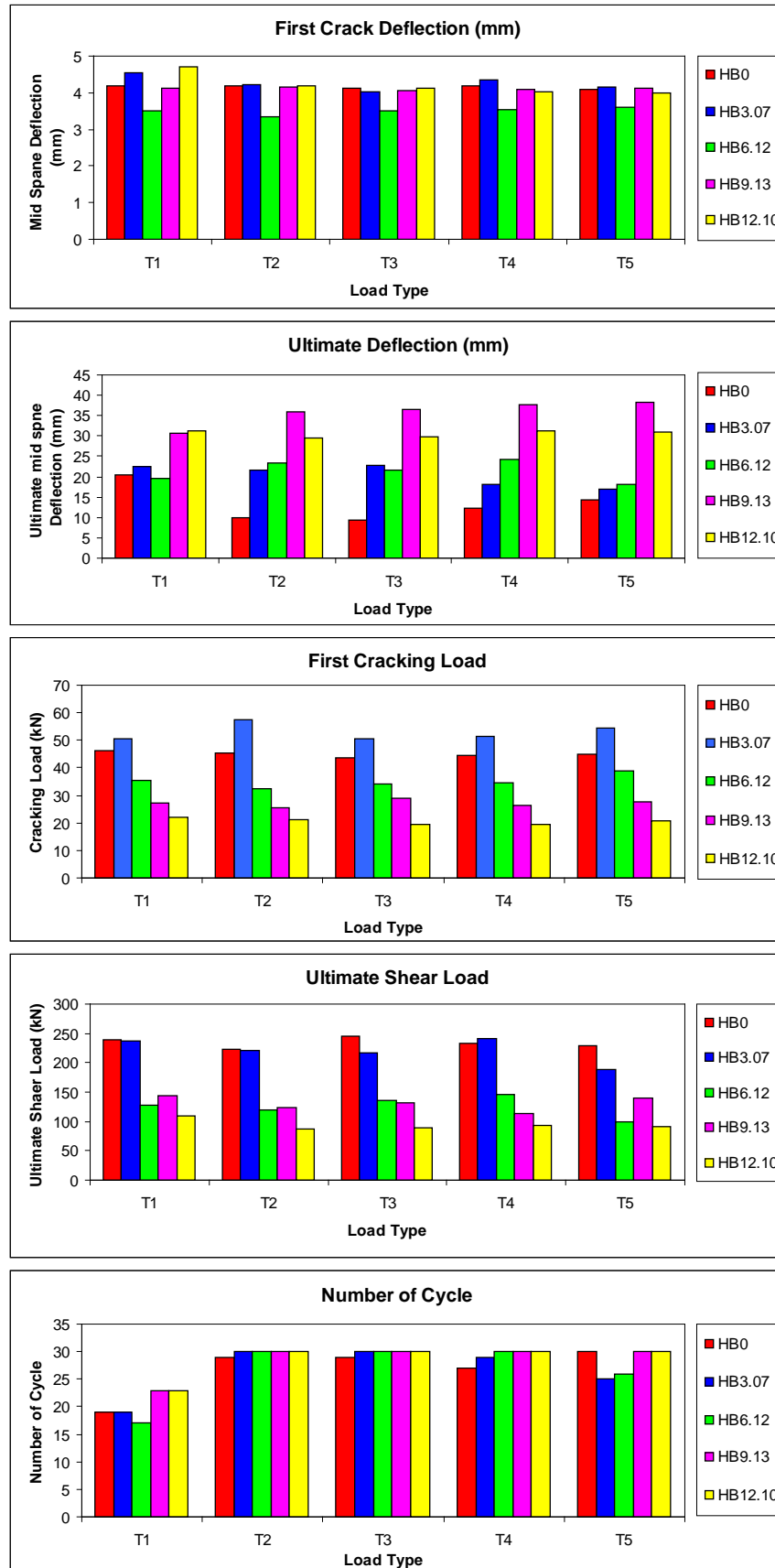


Figure (14): Comparisons between load histories Type 1, Type 2, Type 3, Type 4, and Type 5 for each specimen.

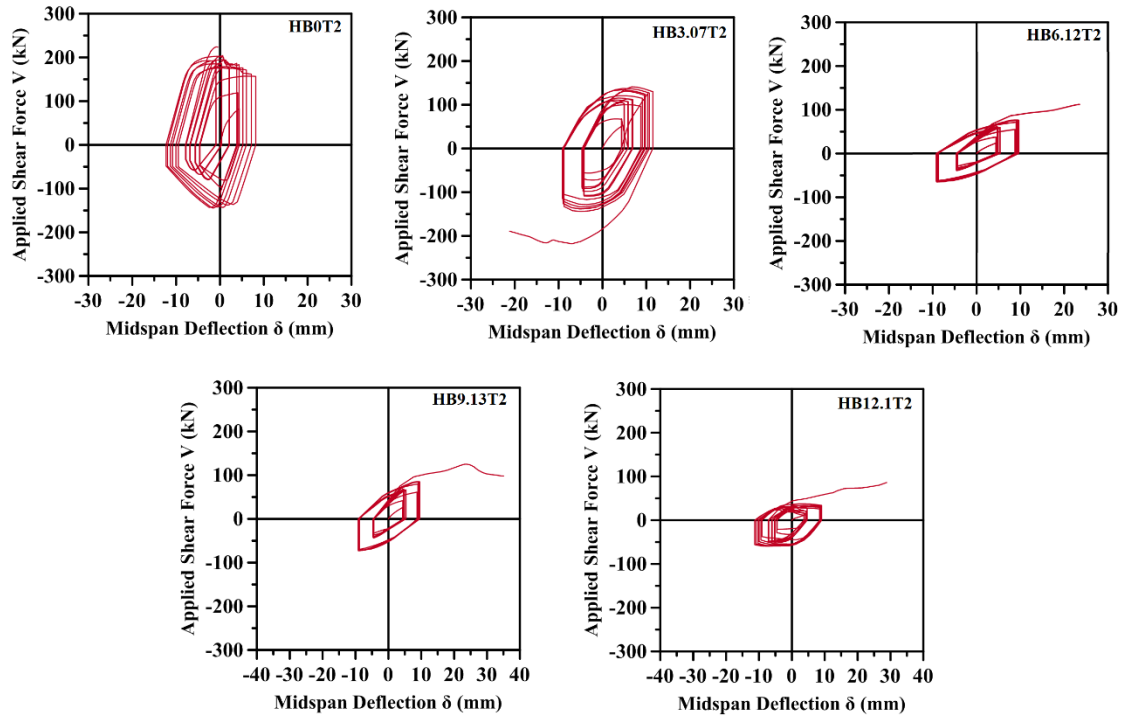


Figure (15): Numerical hysteretic curves for beams tested under (load history 2).

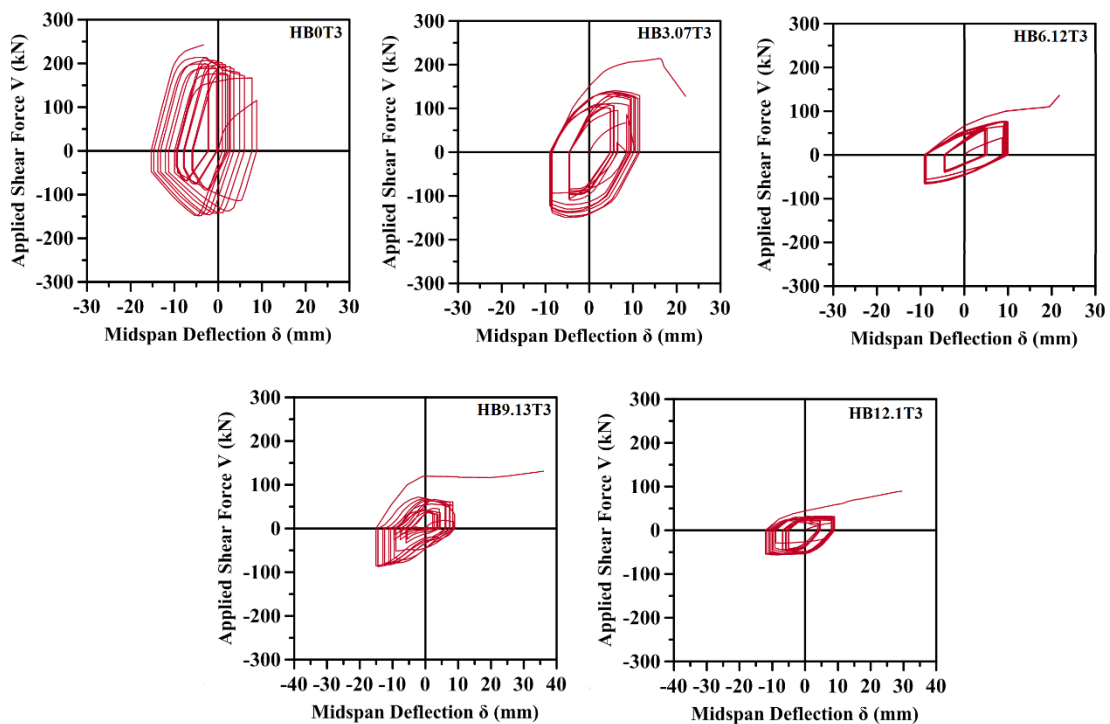


Figure (16): Numerical hysteretic curves for beams tested under (load history 3).

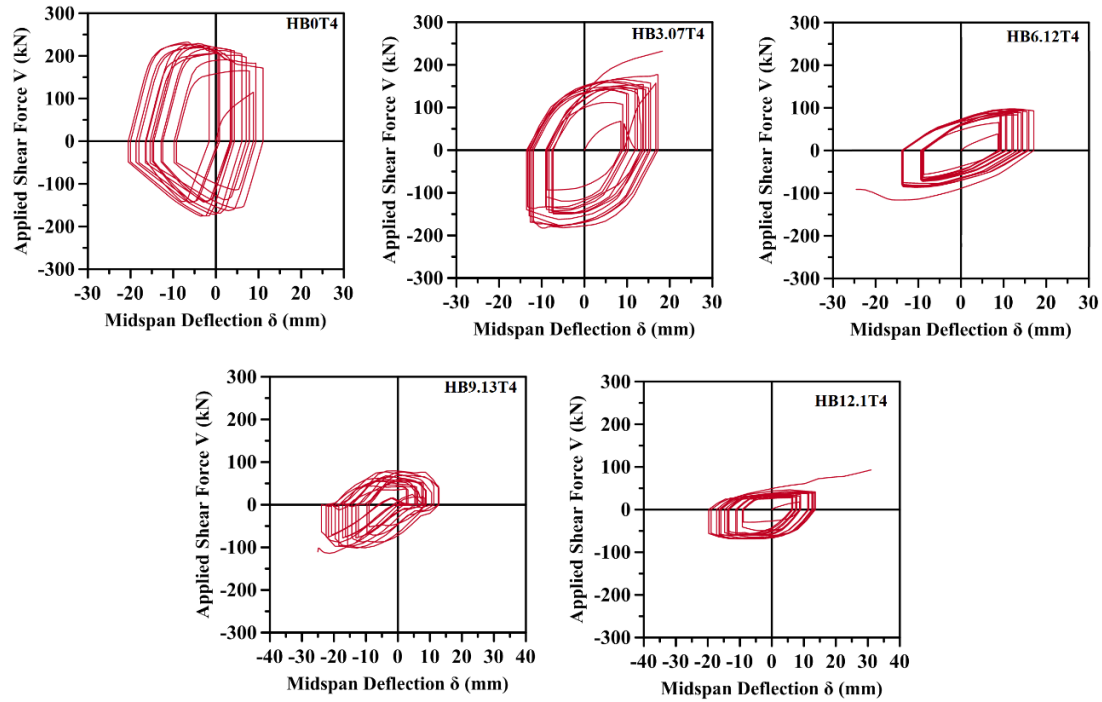


Figure (17): Numerical hysteretic curves for beams tested under (load history 4).

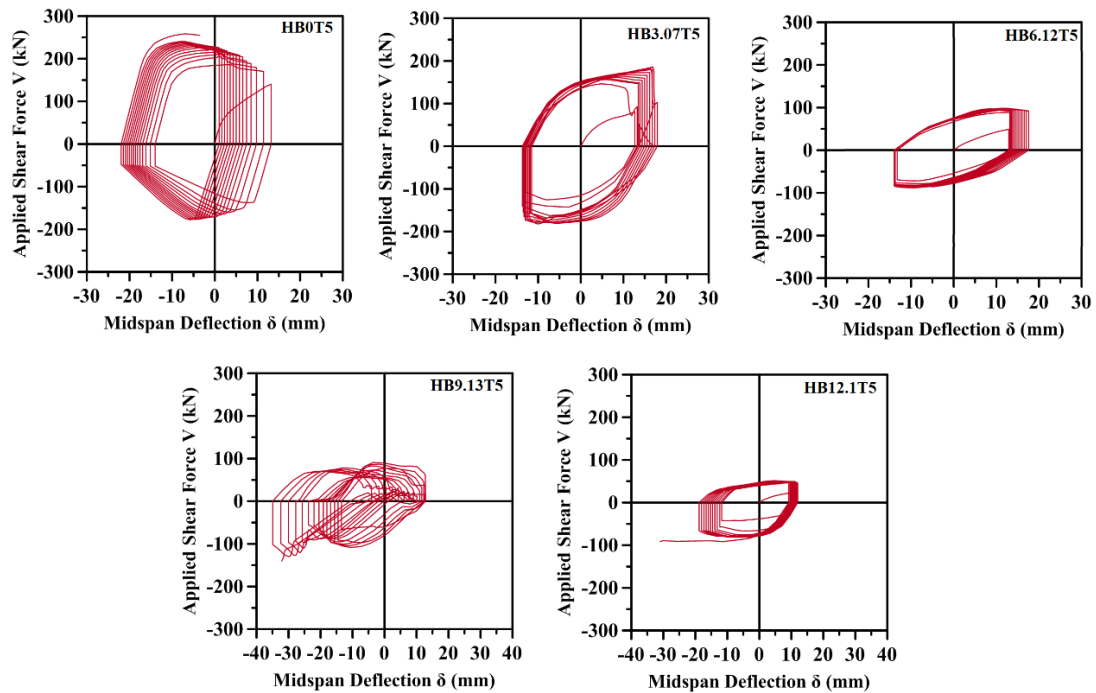


Figure (18): Numerical hysteretic curves for beams tested under (load history 5).

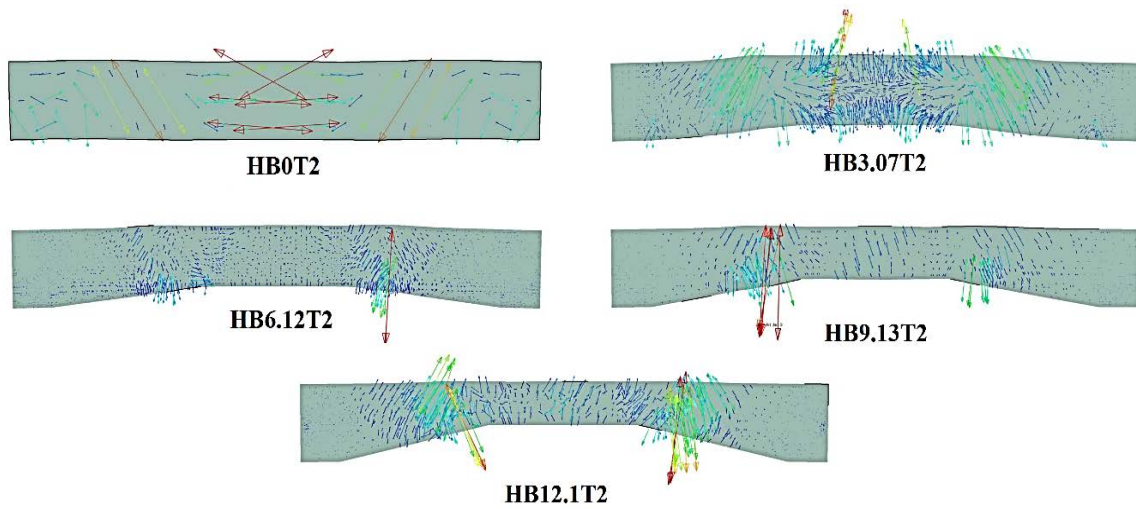


Figure (19): Numerical crack patterns for load type 2.

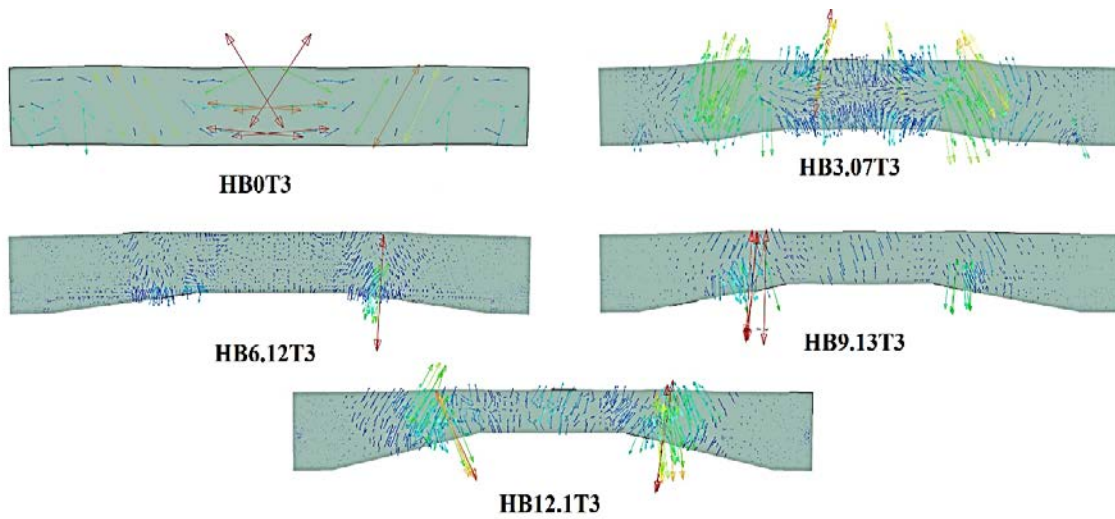


Figure (20): Numerical crack patterns for load type 3.

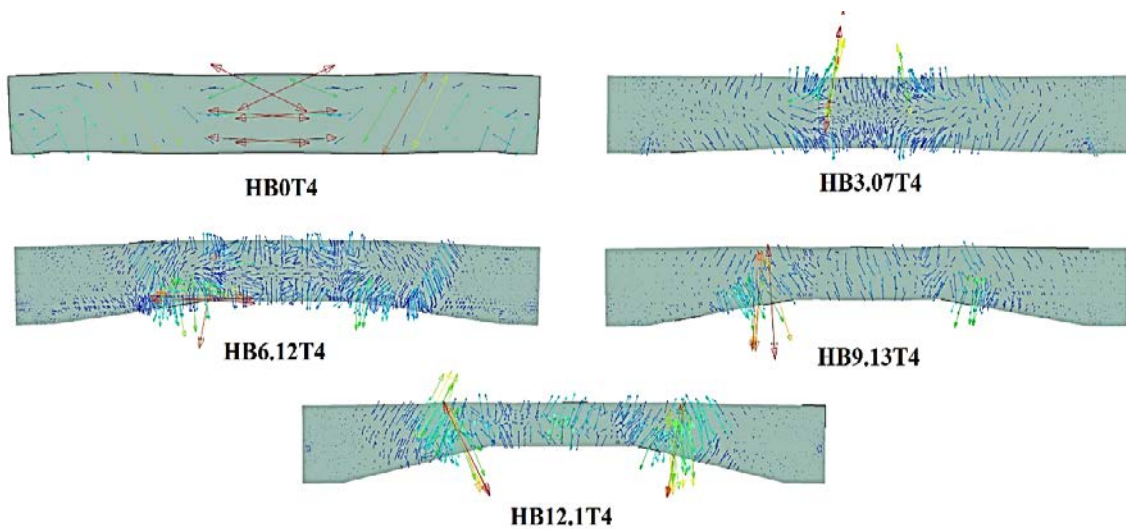


Figure (21): Numerical crack patterns for load type 4.

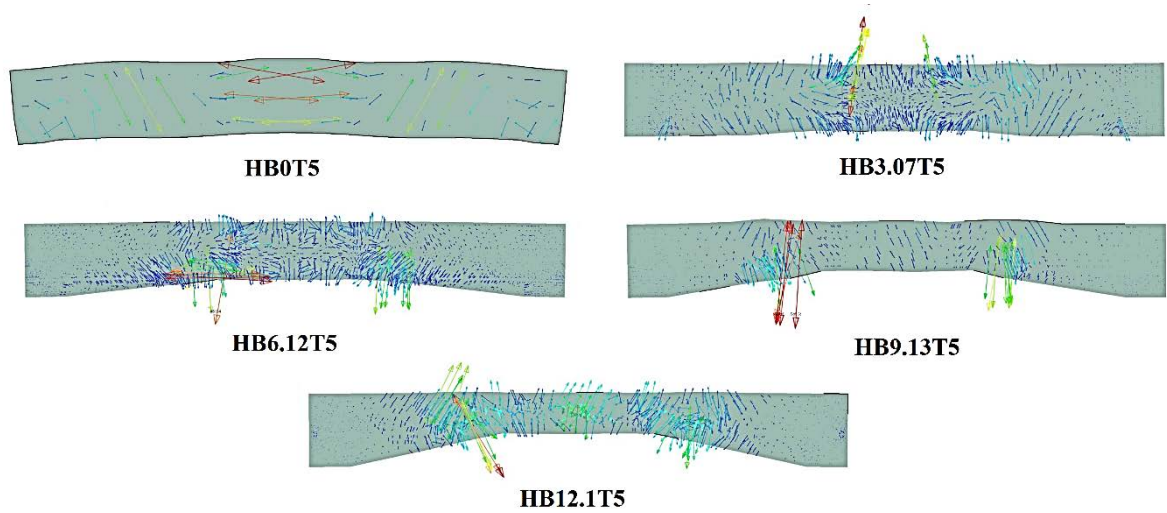


Figure (22): Numerical crack patterns for load type 5.

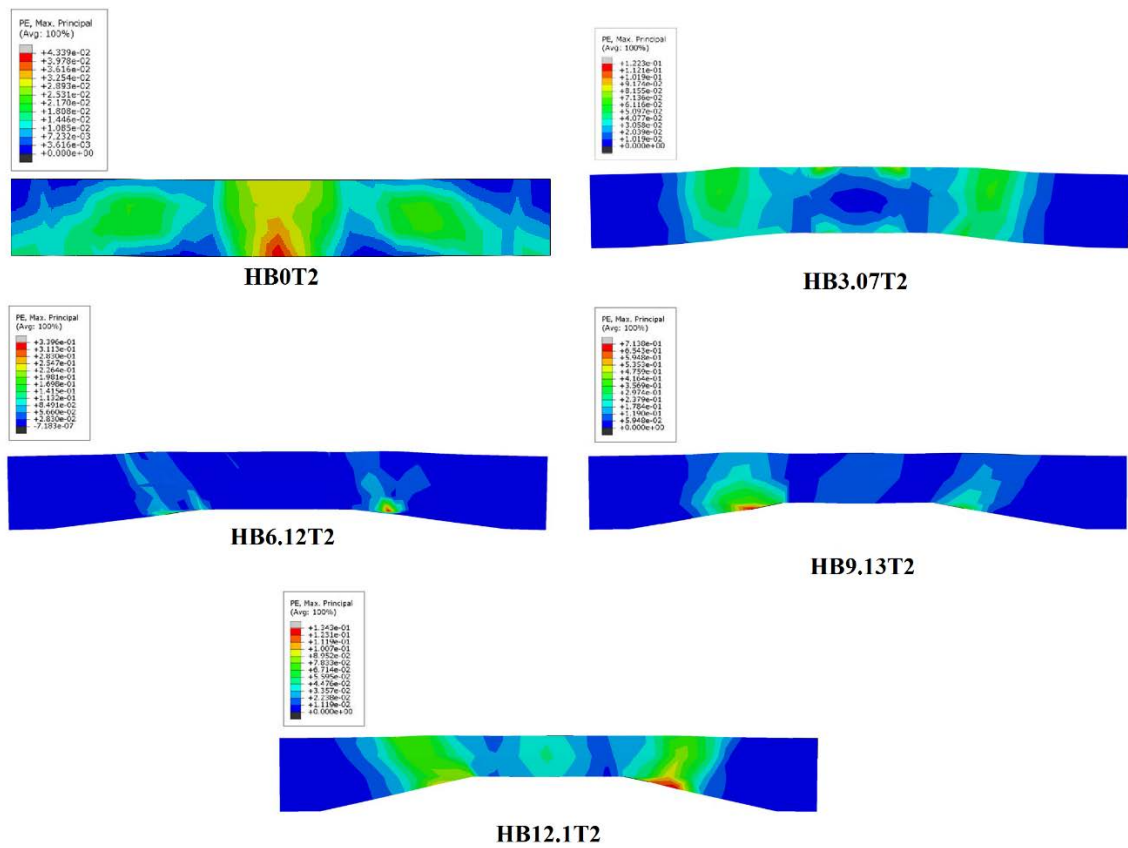


Figure (23): Numerical plastic strain in concrete at ultimate load for load type 2.

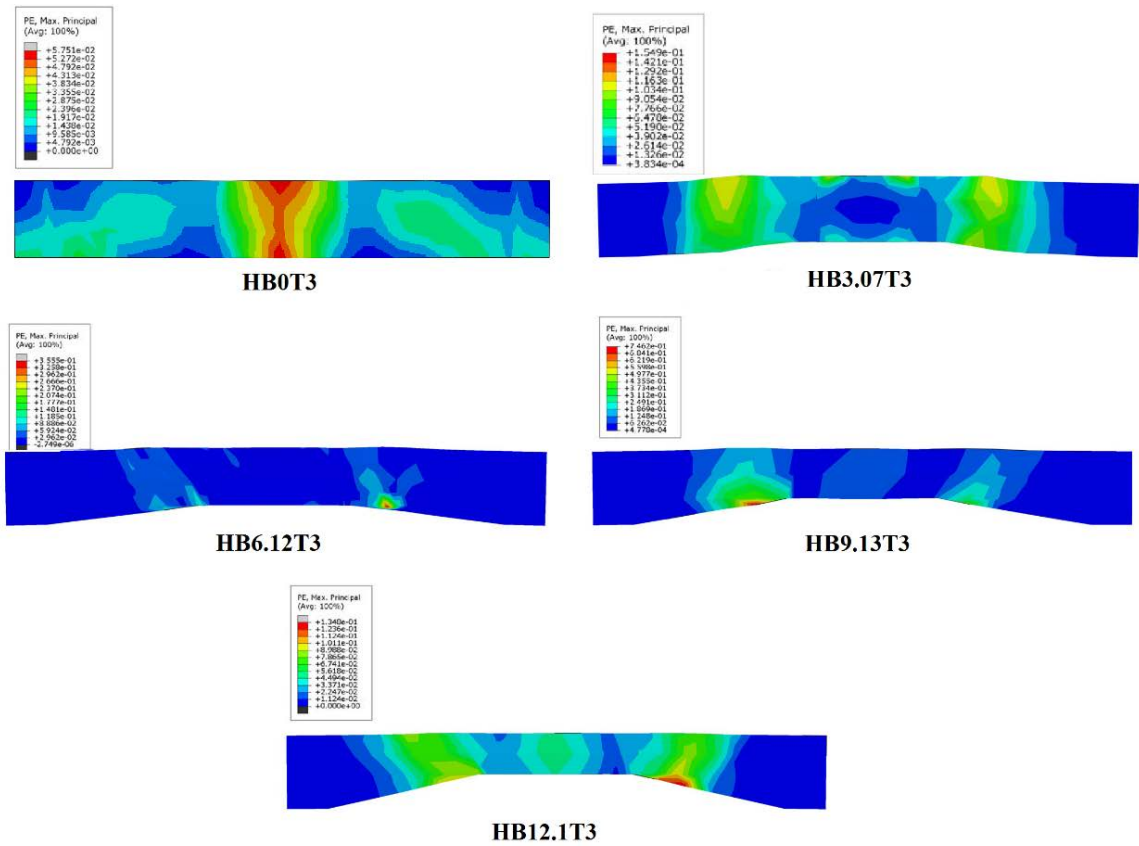


Figure (24): Numerical plastic strain in concrete at ultimate load for load type 3.

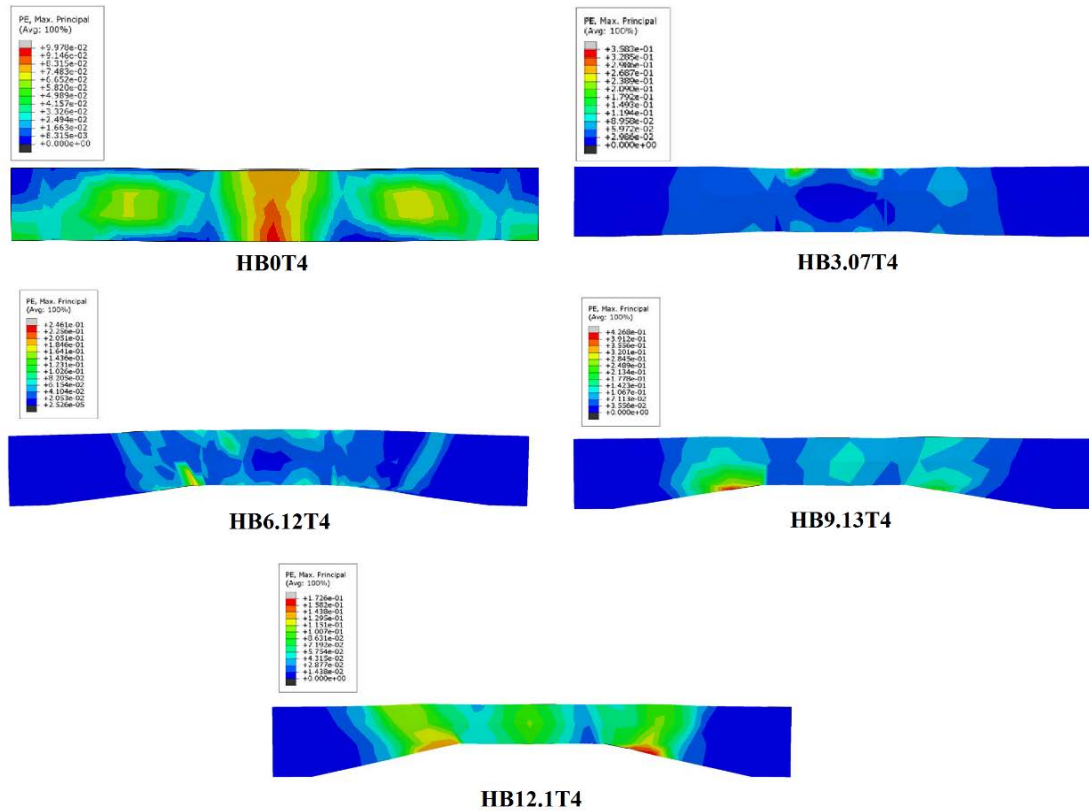


Figure (25): Numerical plastic strain in concrete at ultimate load for load type 4.

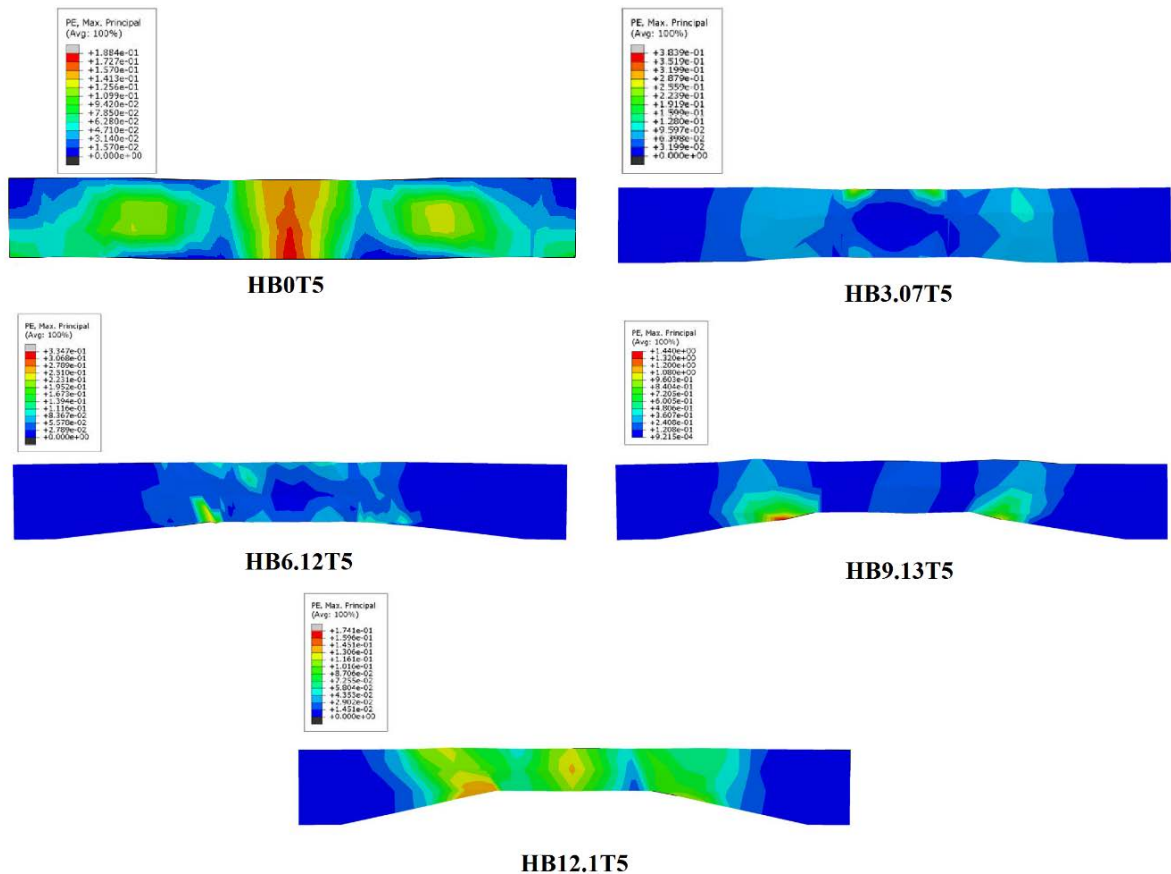


Figure (26): Numerical plastic strain in concrete at ultimate load for load type 5.

8. Concluding Remarks

The first part of this study focused to calibrate the finite element analysis with experimental results by applying load history Type 1 which represents the experimental program by Aranda et al. [1]. From the results of numerical analysis and a comparison with experimental results, the following concluding remarks were observed:

1. A good correlation between experimental and numerical hysteretic loops exists for the five beam specimens under load Type 1.
2. A good agreement of numerical ultimate shear load (V_u) and the corresponding ultimate mid span deflection (Δ_u) which they decreased by 4 and increased by 3 percent respectively (in average) compared with experimental results.
3. A less agreement of numerical number of cycles which decreased by 33 percent (in average) and numerical first cracking shear load and the corresponding deflection (Δ_{cr}) which they decreased by 19.5 and 37.5 percent respectively (in average) than experimental values.
4. A well estimated of numerical cracks patterns, damages and positions of a plastic hinge zone compared to the experimental results.

From the second part of this study which focused to studying the effects of variations in loading history to the response of RCHBs under various cyclic shear loading histories and a comparisons between load histories Type 1, Type 2, Type 3, Type 4, and Type 5the following concluding remarks were observed:

1. No significant change in the numerical first cracking shear load (V_{cr}) and the corresponding deflection (Δ_{cr}) for the five beam specimens under various loading histories.
2. A significant change in the ultimate shear load (V_u) from numerical analysis for various loading histories and the corresponding ultimate deflection (Δ_u), which they decreased by 7.9 and 5.52 percent respectively (in average) compared to load histories Type 1.
3. A significant change in the numerical number of cycles at ultimate load which increased by 46 percent (in average) for various loading histories compared to load histories Type 1.
4. Numerical cracks patterns, damages and position of plastic hinge zone for the five beams were similar to the results of five beams under load histories Type 1.

9. References

- [1] Archundia-Aranda HI, Tena-Colunga A, Grande-Vega A. "Behavior of reinforced concrete haunched beams subjected to cyclic shear". Eng. Struct. 2013; 49: 27–42.
- [2] Lubliner, J., Oliver, J., Oller, S., and Onate, E., "A plastic-damage model for concrete", Solids and Structures J, 1989, Vol. 25, No. 3, pp. 299-326.
- [3] Lee, J., and Fenves, G., "Plastic-damage model for cyclic loading of concrete structure", Engineering Mechanics J, 1998, Vol. 124, No. 8, pp. 892-900.
- [4] Thorenfeldt, E., Tomaszewicz, A., and Jensen, J, "Mechanical properties of high-strength concrete and applications in design," in Proc. Symp. Utilization of High-Strength Concrete, (Stavanger, Norway), 1987.
- [5] Hordijk, D., Local approach to fatigue of concrete. PhD thesis, Delft University of Technology, Delft, The Netherlands, 1991.
- [6] Menegotto, M. and Pinto, E., "Method of analysis for cyclically loaded reinforced concrete plane frames including changes in geometry and non-elastic behavior of elements under combined normal force and bending," in IABSE Symposium on the Resistance and Ultimate Deformability of Structures Acted on by Well-Defined Repeated Loads, (Lisbon), 1973.
- [7] ABAQUS, ABAQUS/standard, version 6.8, ABAQUS, Inc., Pawtucket, R.I, 2009.
- [8] Oller, S., Onate, E., Oliver, J. and Lubliner, J., "Finite Element Nonlinear Analysis of Concrete Structures using a 'Plastic-Damage Model' ", Engineering Fracture Mechanics, Vol. 35, 1990, pp. 219-231.
- [9] ACI Committee 318, "Building Code Requirements for Structural Concrete (ACI 318M-11) and Commentary", American Concrete Institute, Farmington Hills, MI 48331, USA, 2011.
- [10] CEB-FIP, Model Code 1990, Design code. Lausanne, Switzerland: Thomas Telford, 1993.
- [11] Rummel, G., "Zumzug und Schubtragverhalten von bauteilenaushochfestbeton," tech. rep., Deutscher Ausschuss für Stahlbeton, Beuth Verlag, Berlin, Germany, 1994.
- [12] Monti, G. and Nuti, C., "Nonlinear cyclic behavior of reinforcing bars including buckling," ASCE Journal of Structural Engineering, vol. 118, no. 12, p. 32683284, 1992.
- [13] Tuo, L., Jiang, Q., & Chengqing, L. (2008). Application of damaged plasticity model for concrete. Structural Engineers, 24(2), 22–27
- [14] Xue, Z., Yang, L., and Yang, Z. (2010). A damage model with subsection curve of concrete and its numerical verification based on ABAQUS. In: 2010 International Conference On Computer Design And Applications (ICDA 2010) (Vol. 5, pp. 34–37.
- [15] Garg, A.K., Abolmaali, A., "Finite-Element modeling and Analysis of Reinforced Concrete Box Culverts", Journal of Transportation Engineering, Vol. 135, No. 3, 2009, ASCE, pp. 121-128.
- [16] Rahai, A., Hatami, F., "Evaluation of composite shear wall behavior under cyclic loadings", J. Constr. Steel Res., Vol. 65, 2009, pp. 1528-1537.
- [17] Deng, S., Qie, Z., Wang, L., "Nonlinear Analysis of Reinforced Concrete Beam Bending Failure Experimentation Based on ABAQUS", International Conference on Information Sciences, Machinery, Materials and Energy (ICISMME 2015).

التحليل بواسطة العناصر المحددة للعتبات الخرسانية متغيرة المقطع تحت تأثير الاحمال المتكررة

عبد الخالق جبار عبد الرضا
كلية الهندسة
جامعة النهريين

ابراهيم سليم ابراهيم حربيه
كلية الهندسة
جامعة النهريين

الخلاصة

تظهر هذه الدراسة المحاكاة التحليلية باستخدام العناصر المحددة لدراسة تأثير تسليط الانماط المختلفة من الاحمال المتكررة على سلوك العتبات متغيرة المقطع. ضمن محاور هذا البحث تم تمثيل خمس عتبات متغيرة المقطع من الخرسانة المسلحة باستخدام نموذج العناصر المحددة المتوفرة في برنامج ABAQUS. حيث تم استخدام نموذج التضرر اللدن لتمثيل الخرسانة تحت تأثير الاحمال المحورية المتكررة في الانضغاط والشد. تم تقسيم الدراسة الى محورين المحور الاول يتضمن مقارنة نتائج المحاكاه النظرية مع النتائج العملية تم اختيارها للتأكد من امكانية التحليل بواسطة العناصر المحددة. واطهرت المقارنة تطابق جيد. اما المحور الثاني من الدراسة تم تسليط اربعة انواع مختلفة من الاحمال المتكررة لدراسة تأثيرها على سلوك العتبات متغيرة المقطع. اظهرت النتائج ان تأثير تغير الاحمال يسبب زيادة عدد دورات التحميل ونقصان في التحمل الاقصى للعتبات ونقصان في الهطول.